


Hydrophobic Surface Enhances Electrostatic Interaction in Water

Takato Sato,¹ Tohru Sasaki,¹ Jun Ohnuki,¹ Koji Umezawa,² and Mitsunori Takano^{1,*}

¹*Department of Pure and Applied Physics, Waseda University, Ohkubo 3-4-1, Shinjuku-Ku, Tokyo 169-8555, Japan*

²*Department of Biomedical Engineering/Institute for Biomedical Sciences, Shinshu University, 8304 Minami-minowa, Kami-ina, Nagano, 399-4598, Japan*

 (Received 17 August 2018; published 15 November 2018)

A high dielectric constant is one of the peculiar properties of liquid water, indicating that the electrostatic interaction between charged substances is largely reduced in water. We show by molecular dynamics simulation that the dielectric constant of water is decreased near the hydrophobic surface. We further show that the decrease in the dielectric constant is due to both the decreased water density and the reduced water dipole correlation in the direction perpendicular to the surface. We finally demonstrate that electrostatic interaction in water is actually strengthened near the hydrophobic surface.

DOI: [10.1103/PhysRevLett.121.206002](https://doi.org/10.1103/PhysRevLett.121.206002)

Liquid water possesses unusual physical properties. Among them is its high dielectric constant [1,2], meaning that the electrostatic attraction or repulsion between charged substances should be largely reduced in water. In contrast, the hydrophobic interaction, which reflects another aspect of the unusual physical properties of water, is certainly one of the major attractive forces in water, and its microscopic origin has long been studied [3–9]. Which interaction, electrostatic or hydrophobic, is dominant in water has often been controversial, particularly when biological molecules are involved, because those molecules, such as proteins, are a complex mosaic of hydrophilic and hydrophobic substances, utilizing the electrostatic interaction as well [10,11]. Interestingly, recent experimental studies have suggested that these two interactions are intimately related to each other [12,13]; particularly, Chen *et al.* showed that the electrostatic attraction in water is strengthened near the hydrophobic surface [13].

Schellman pointed out early, employing the method of image charges, that the hydrophobic surface can strengthen the electrostatic attraction in water [14]. While Schellman assumed that the dielectric constant of water is spatially uniform, the existence of the hydrophobic surface would disturb the nearby hydrogen bond network of water molecules and make the dielectric constant nonuniform. Actually, the decrease in the dielectric constant near the hydrophobic surface was suggested theoretically [15] and experimentally [16]. The decrease in the dielectric constant for the interfacial water has also been observed in molecular dynamics simulations [17–20]. Recently, Fumagalli *et al.* demonstrated by capacitance microscopy that the dielectric constant of water is considerably lowered near a graphite surface [21].

The physical mechanism for the decrease in the dielectric constant near the hydrophobic surface, however, remains unclear, even though it has often been envisaged that an

icelike structure formation near the hydrophobic surface, as often envisaged in the hydrophobic interaction [3], would reduce the dielectric susceptibility [13,16,21]. In this Letter, by conducting molecular dynamics (MD) simulation, we systematically investigate the dielectric constant and other fundamental physical properties of water around well-defined hydrophobic surfaces, and we elucidate the physical mechanism for the decrease in the dielectric constant near the hydrophobic surface. We further demonstrate that the decreased dielectric constant leads to an enhancement of the electrostatic interaction near the hydrophobic surfaces.

As an ideal hydrophobic substance, we considered a particle that interacts with water molecules only via the Weeks-Chandler-Andersen (WCA) potential [22]. The WCA potential is a modified Lennard-Jones (LJ) potential where the interaction is truncated at the distance where the potential becomes the minimum, i.e.,

$$U(r) = \begin{cases} 0 & (r > r_0) \\ \epsilon_{\text{LJ}}[1 - 2(\frac{r_0}{r})^6 + (\frac{r_0}{r})^{12}] & (r \leq r_0), \end{cases} \quad (1)$$

where r represents the center-to-center distance between the particle (which we hereafter refer to as “WCA particle”) and the oxygen atom of a water molecule. We employed the LJ parameters for the methane-water interaction ($r_0 = 0.387$ nm and $\epsilon_{\text{LJ}} = 0.896$ kJ/mol) [23]. The radius of the WCA particle, which determines the surface of the WCA particle, is defined by $r_0 - \frac{1}{2}r_w$, where r_w represents the LJ parameter for the water-water interaction (0.355 nm) [24]. The radius of the WCA particle can be changed by using a shifted $U(r)$ [the radius is increased by R_s by using $U(r - R_s)$], as was employed by Sarupria and Garde [23]. In this study, we first considered a WCA particle with a radius 2 nm ($R_s = 1.8$ nm), which corresponds to the radius of gyration for a protein molecule composed of

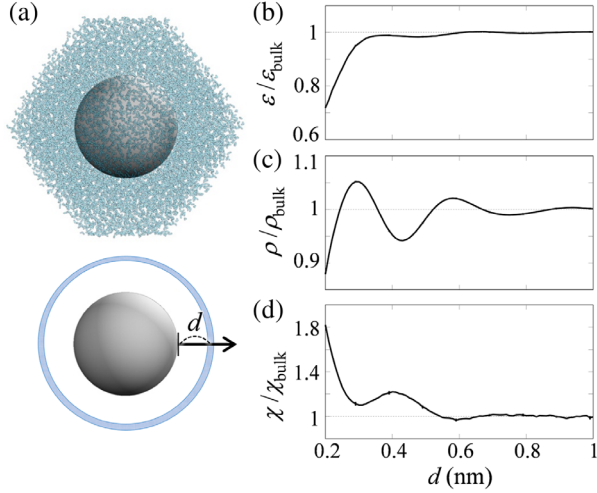


FIG. 1. (a) WCA particle-water system: a WCA particle with a radius 2 nm is immersed in a truncated octahedron (trimmed-down cube) unit cell containing 8667 water molecules. (b)–(d) Physical properties of water were calculated as a function of the distance from the surface of the WCA particle in the radial direction (denoted by d): (b) (relative) dielectric constant ϵ , (c) number density ρ , and (d) isothermal compressibility $\chi \equiv V\langle\Delta\rho^2\rangle/k_{\text{B}}T\rho^2$ (V is the volume of the spherical shell with 0.1 nm width). The values are normalized by the averages in the bulk water region ($0.8 \leq d \leq 1.0$ nm): $\epsilon_{\text{bulk}} = 32.9$ (for this value, see text and Fig. S1 [29]), $\rho_{\text{bulk}} = 33.7 \text{ nm}^{-3}$, $\chi_{\text{bulk}} = 4.2 \text{ GPa}^{-1}$. Error bars represent the 95% confidence interval (estimated from four MD runs).

~300 amino-acids [25]. As shown in Fig. 1(a), the WCA particle was immersed in a unit cell filled with SPC/E (extended simple point charge model) waters [24], to which the periodic boundary condition and the particle mesh Ewald method [26] was applied. The temperature and the pressure of the system were set at 300 K and 0.1 MPa, respectively, and the time step was set at 2 fs by fixing the bond lengths involving hydrogen atoms [27]. We carried out four independent 6-ns MD simulations using AMBER9 [28] with modification to implement the WCA potential.

We first investigated the local dielectric constant of water around the WCA particle, using the Onsager-Kirkwood-Fröhlich formula [30–32],

$$\frac{(\epsilon(\mathbf{x}) - 1)(2\epsilon(\mathbf{x}) + 1)}{3\epsilon(\mathbf{x})} = \frac{\langle\Delta\boldsymbol{\mu}(\mathbf{x})^2\rangle}{4\pi\epsilon_0 k_{\text{B}} T a^3}, \quad (2)$$

where $\epsilon(\mathbf{x})$ indicates the local (relative) dielectric constant that is calculated from the thermal fluctuation of the *total* water dipole moment $\boldsymbol{\mu}$ in a probing sphere with radius a centered at \mathbf{x} ; we set a at a small value of 0.2 nm to study the local dielectric constant. The bracket indicates the statistical average using the data sampled at 2 ps interval, and Δ indicates the instantaneous deviation from the average (k_{B} is the Boltzmann constant and T is the temperature). The dielectric constant as a function of d

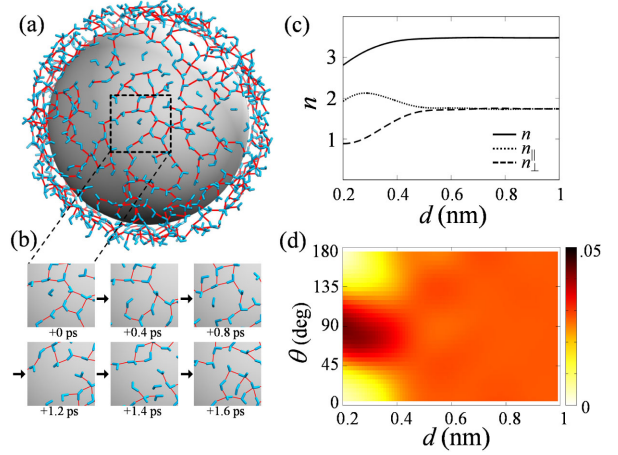


FIG. 2. Hydrogen bond (H-bond) network of water molecules around the WCA particle. (a) A snapshot of a H-bond network formed within the first hydration shell ($d \leq 0.42$ nm), and (b) an example of the network rearrangement dynamics observed in the dotted square in (a). H-bonds are shown in magenta. (c) Average number of H-bonds per water molecule (denoted by n) as a function of d (the distance from the surface of the WCA solute). The H-bond was defined to be formed when $\text{H}\cdots\text{O}$ and $\text{O}\cdots\text{O}$ distances are less than 0.24 and 0.36 nm, respectively, and the angle formed by $\text{O}-\text{H}$ and $\text{O}\cdots\text{O}$ is less than 30° [35]. The H-bond was defined to be parallel to the surface when the angle between the H-bond ($\text{H}\cdots\text{O}$) and the radial axis falls within $90 \pm 30^\circ$; the number of the H-bonds parallel to the surface is denoted by n_{\parallel} and that perpendicular to the surface by n_{\perp} . (d) Probability density distribution of the angle between the water dipole vector and the radial axis (denoted by θ). $\theta > 90^\circ$ when the dipole vector points toward the surface.

(the distance from the surface of the WCA particle) is shown in Fig. 1(b). We can find that ϵ is decreased near the surface of the WCA particle. In Figs. 1(c) and 1(d), the number density of water, ρ , and the isothermal compressibility, χ , are shown. A decrease in ρ is seen near the surface of the WCA particle, known as “dewetting” [6]. In addition, a thermal fluctuation of ρ is enhanced near the surface, which is reflected in the increase in χ , as was previously observed [23,33]. Thus, the property of water near the surface of the WCA particle is vaporlike (i.e., lower density and higher compressibility), which partly accounts for the decrease in ϵ . Note that, the saturated value of ϵ is smaller than the value expected for bulk water [34], because in this study, ϵ was evaluated in a small probing sphere to obtain local dielectric constants (it is shown in Fig. S1 [29] that the saturated value of ϵ increases with increasing a , while the relative decrease in ϵ near the surface remains unchanged).

We then looked into the structural properties of water around the WCA particle, focusing on the hydrogen bond (H-bond) network. In Fig. 2(a), a typical snapshot of the water molecules in the first hydration shell ($d \leq 0.42$ nm) and the H-bonds formed among them are shown. While a large-scale H-bond network can be found, it is rather patchy

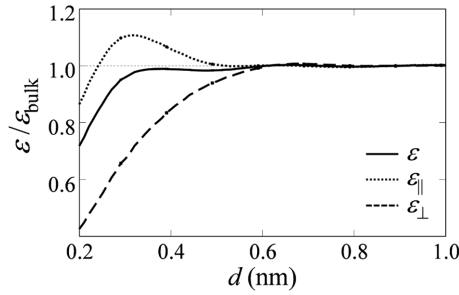


FIG. 3. Direction dependence of the dielectric constant of water around the WCA particle. The component parallel to the surface of the WCA particle, $\epsilon_{||}$, and that perpendicular to the surface, ϵ_{\perp} , are shown as a function of d . The values are normalized by the averages in the bulk water region ($0.8 \leq d \leq 1.0$ nm) ($\epsilon_{\text{bulk}} = 32.9$, $\epsilon_{||\text{bulk}} = 32.9$, $\epsilon_{\perp\text{bulk}} = 32.9$).

and fragile, exhibiting extensive network rearrangement on the picosecond time scale [Fig. 2(b)]. The fragility of a H-bond near the surface is also seen in the decrease in the number of H-bonds, n [Fig. 2(c)]. The decrease in n is caused by the decrease in n_{\perp} (the number of H-bonds perpendicular to the surface). The decrease in n is partially recovered by the increase in $n_{||}$ (the number of H-bonds parallel to the surface); consistent with this, the water molecules in the first hydration shell tend to orient their dipole vectors parallel to the surface [Fig. 2(d)].

The observed directional preference of the H-bonds and the water dipoles should affect the dielectric response of water, as was previously observed in MD simulations [18,19,36,37]. We then calculated the components of the dielectric constant parallel to and perpendicular to the surface of the WCA particle, denoted by $\epsilon_{||}$ and ϵ_{\perp} , respectively, by the following equation [17],

$$\frac{(\epsilon_{\alpha}(\mathbf{x}) - 1)(2\epsilon_{\alpha}(\mathbf{x}) + 1)}{3\epsilon_{\alpha}(\mathbf{x})} = \frac{\langle \Delta\mu(\mathbf{x})_{\alpha}^2 \rangle}{4\pi\epsilon_0 k_B T a^3}, \quad (3)$$

where α designates “||” or “⊥”, and $\Delta\mu_{\perp}^2 = (\Delta\mu \cdot \mathbf{e}_r)^2$ and $\Delta\mu_{||}^2 = \frac{1}{2}[(\Delta\mu \cdot \mathbf{e}_{\theta})^2 + (\Delta\mu \cdot \mathbf{e}_{\phi})^2]$, with \mathbf{e}_r , \mathbf{e}_{θ} , and \mathbf{e}_{ϕ} being the polar coordinate unit vectors at \mathbf{x} . In Fig. 3, $\epsilon_{||}$ and ϵ_{\perp} are shown as a function of d . As expected, ϵ near the surface of the WCA particle shows clear directionality; $\epsilon_{||}$ is increased, whereas ϵ_{\perp} is decreased compared to the bulk value. It is noteworthy that the decrease in ϵ_{\perp} reaches farther than that of ϵ . Therefore, the decrease in the dielectric constant near the surface is caused not only by the decreased water density but by the weakened water dipole correlation in the perpendicular direction (remember that μ is the sum of the dipole moments of water molecules in the probing sphere).

Here, we mention the effect of the size of the WCA particle [6]. As shown in Fig. S2(a) [29], for a small-sized WCA particle of radius 0.2 nm (corresponding to the size of a methane molecule), ϵ is not decreased but increased near

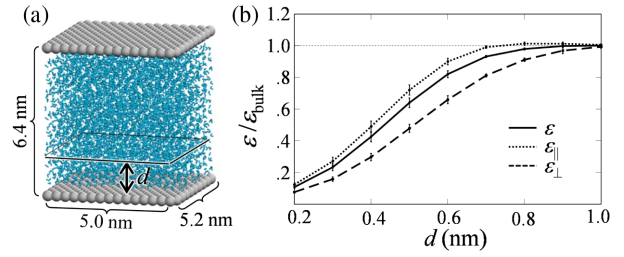


FIG. 4. (a) WCA plane-water system: the WCA plane is composed of close-packed 270 WCA particles. Two WCA planes sandwich 5019 water molecules (6.4 nm thickness), and each WCA particle in the planes was fixed at its original position. Outer regions of the planes are a vacuum (7.5 nm thickness each), resulting in a rectangular unit cell of 5.0 nm \times 5.2 nm \times 21.4 nm, to which the periodic boundary condition and the particle mesh Ewald method [26] were applied. The simulation procedure was the same as in the WCA particle-water system, and eight independent 2-ns simulations were conducted at the constant volume condition at 300 K after 0.5 ns equilibration at 0.1 MPa. (b) Dielectric constant of water as a function of d (the distance from the surface of the WCA plane). Parallel and perpendicular components to the WCA plane, $\epsilon_{||}$ and ϵ_{\perp} , are also shown. The values are normalized by the averages in the bulk water region ($1.2 \leq d \leq 1.4$ nm): $\epsilon_{\text{bulk}} = 32.1$, $\epsilon_{||\text{bulk}} = 32.0$, $\epsilon_{\perp\text{bulk}} = 32.5$.

the WCA particle. This is due to the increased number density [Fig. S2(b)] and the increased water dipole correlation near the particle, which is caused by the strengthened H-bonds [see the increased H-bond lifetime near the surface as shown in Fig. S2(d)]. For a medium-sized WCA particle of radius 1 nm (corresponding to the size of a protein molecule with ~ 50 amino acids [25]), the decrease in ϵ is again observed near the surface [Fig. S2(a)]; the profiles of the other physical properties [Figs. S2(b)–(c)] also become similar to those observed in the large-sized WCA particle of radius 2 nm.

We then considered a “WCA plane” composed of close-packed small-sized WCA particles as shown in Fig. 4(a) [the size of the WCA particle was set to that of a water molecule ($r_0 = 0.355$ nm, $\epsilon_{\text{LJ}} = 0.650$ kJ/mol [24])]. As seen in Fig. 4(b), the decrease in the dielectric constant is observed near the surface of the WCA plane (we defined the surface of the WCA plane as the common tangential plane to the surfaces of the WCA particles). Furthermore, the region with decreased ϵ extends as far as $d \sim 1$ nm. In this case, the region with $\epsilon_{||}$ larger than the bulk value, as seen in Fig. 3, almost disappears due to the enhanced dewetting [Fig. S3(a) [29]]. That ϵ_{\perp} is lower than $\epsilon_{||}$ indicates the weakened water dipole correlation in the perpendicular direction.

From the observed decrease in the dielectric constant, we expect that the electrostatic interaction is strengthened near the hydrophobic surface, compared to that in bulk water. To see this, we calculated the potential of mean force (PMF) between two charged particles in the WCA plane-water system [Fig. 5(a)]: one is a WCA particle in the WCA plane

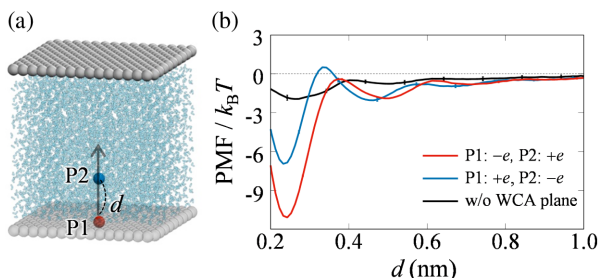


FIG. 5. (a) The same WCA plane-water system as shown in Fig. 4(a) except that one WCA particle in the plane ($P1$) is charged and another WCA particle ($P2$), with the opposite charge, is placed above $P1$ (the z axis passing through the mass centers of $P1$ and $P2$ is perpendicular to the surface of the WCA plane). (b) Potential of mean force (PMF) between $P1$ and $P2$ as a function of d (the distance from the surface of $P1$ to the center of $P2$): (red) $P1$ charged with $-e$ and $P2$ with $+e$; (blue) $P1$ with $+e$ and $P2$ with $-e$. The umbrella sampling was conducted by applying the umbrella potential $K(\zeta - \zeta_0)^2$ to $P1$ and $P2$; ζ is the center-to-center distance between $P1$ and $P2$ and ζ_0 was shifted from 0.378 to 0.678 nm at the interval of 0.015 nm with $K = 6.3 \times 10^3$ kJ/mol/nm² and from 0.678 to 1.578 nm at the interval of 0.05 nm with $K = 6.3 \times 10^2$ kJ/mol/nm². Restoring force to place $P2$ on the z axis was applied to $P2$ with the force constant of 4.2×10^4 kJ/mol/nm². PMF is given by $-k_B T \ln p(\zeta)$, where $p(\zeta)$ is the equilibrium probability distribution obtained by the weighted histogram analysis method [38]. For comparison, PMF between $P1$ and $P2$ calculated in bulk water (i.e., without the WCA planes and vacuum regions) is shown (black). PMF was adjusted so that the average in the large d region ($1.2 \leq d \leq 1.4$ nm) becomes zero.

(referred to as “ $P1$ ”) to which an electric charge is added, and the other is another WCA particle (referred to as “ $P2$ ”) that is oppositely charged and placed above $P1$ in the water region. In Fig. 5(b), PMFs thus obtained are shown as a function of d for the case where $P1$ has $-e$ and $P2$ has $+e$ (red line) and the case where charges of $P1$ and $P2$ are reversed (blue line). By comparing with the PMF between the oppositely charged $P1$ and $P2$, calculated in bulk water, i.e., in the absence of the WCA planes and vacuum regions (black line), it is clear that the electrostatic attraction is enhanced by the presence of the WCA plane. The enhancement of the electrostatic stabilization becomes largest at $d = 0.24$ nm, and continues to as far as $d \sim 1$ nm, which is coincident with the reach of the decreased dielectric constant as seen in Fig. 4(b). The detailed structure in the PMF comes from the molecular nature of the solvent. Particularly, the minimum at $d = 0.24$ nm is due to the water molecules making electrostatic bonds with $P1$ and $P2$ simultaneously; since the water dipoles near the surface ($d \sim 0.2$ nm) have a slight tendency to point toward the WCA plane [$\theta > 90^\circ$; see Fig. S3(b)], the minimum is raised in the case of positively-charged $P1$. We note that, the enhancement of the electrostatic attraction, even for the positively-charged $P1$, is greater than that calculated by the

method of image charges on the assumption of spatially uniform dielectric constant (see Fig. S4 [29]).

Thus, we showed that the dielectric constant of water is decreased near the hydrophobic surface, in agreement with the recent experiments [13,16,21] and MD simulations [18,20]. We further showed that the decrease in the dielectric constant is caused not only by the decreased water density near the surface but by the reduced water dipole correlation in the direction perpendicular to the surface. As mentioned in the introduction, it has often been hypothesized that water molecules become ordered around the hydrophobic surface by forming icelike structures and the formation of icelike structures results in the reduction of the dielectric susceptibility [13,16,21]. Our MD results do not support this hypothesis; although the formation of H-bonds parallel to the surface is actually enhanced near the hydrophobic surface, it is fragile and hardly viewed as icelike. The physical property of water near the hydrophobic surface is rather vaporlike, as has been highlighted in the context of the hydrophobic interaction [6,8,33].

We then quantitatively showed that the electrostatic interaction is actually enhanced by the presence of the hydrophobic surface, which has recently been suggested by Chen *et al.* [13]. The enhancement of the electrostatic interaction by the hydrophobic surface was early noticed by Schellman [14], and our present study demonstrated that the enhancement can become even greater due to the decrease in the dielectric constant near the surface. In a vacuum, the electrostatic interaction is very strong, and the typical electrostatic interaction energy is much (two orders magnitude) greater than the thermal energy. Water, with its high dielectric constant, can therefore be viewed as an efficient attenuator of the electrostatic interaction, making the electrostatic interaction compatible with the thermal motions [39]. The attenuation of the electrostatic interaction would be particularly important for the biological macromolecules such as proteins; those molecules autonomously undergo association-dissociation dynamics at ambient temperatures. Then the hydrophobic surface can be viewed as a reviver of the electrostatic interaction. The fact that charged amino-acids on protein surfaces are often surrounded by hydrophobic ones [40,41] may indicate that proteins utilize their hydrophobic surfaces to restrengthen the attenuated electrostatic interaction.

We thank Asahi Konno for his contribution in the early stage of this study. This work was supported by Top Global University Project and Grant-in-Aid from MEXT.

*Corresponding author.
mtkn@waseda.jp.

- [1] F. H. Stillinger, *Science* **209**, 451 (1980).
- [2] S. V. Kalinin, *Science* **360**, 1302 (2018).
- [3] W. Kauzmann, *Adv. Protein Chem.* **14**, 1 (1959).

- [4] W. Blokzijl and J. B. F. N. Engberts, *Angew. Chem., Int. Ed. Engl.* **32**, 1545 (1993).
- [5] N. T. Southall, K. A. Dill, and A. D. J. Haymet, *J. Phys. Chem. B* **106**, 521 (2002).
- [6] D. Chandler, *Nature (London)* **437**, 640 (2005).
- [7] R. L. Baldwin, *Proc. Natl. Acad. Sci. U.S.A.* **111**, 13052 (2014).
- [8] E. Xi and A. J. Patel, *Proc. Natl. Acad. Sci. U.S.A.* **113**, 4549 (2016).
- [9] P. Ball, *Proc. Natl. Acad. Sci. U.S.A.* **114**, 13327 (2017).
- [10] F. B. Sheinerman, R. Norel, and B. Honig, *Curr. Opin. Struct. Biol.* **10**, 153 (2000).
- [11] K. Okazaki, T. Sato, and M. Takano, *J. Am. Chem. Soc.* **134**, 8918 (2012).
- [12] C. D. Ma, C. Wang, C. Acevedo-Vélez, S. H. Gellman, and N. L. Abbott, *Nature (London)* **517**, 347 (2015).
- [13] S. Chen, Y. Itoh, T. Masuda, S. Shimizu, J. Zhao, J. Ma, S. Nakamura, K. Okuro, H. Noguchi, K. Uosaki, and T. Aida, *Science* **348**, 555 (2015).
- [14] J. A. Schellman, *J. Phys. Chem.* **57**, 472 (1953).
- [15] F. Despa, A. Fernández, and R. S. Berry, *Phys. Rev. Lett.* **93**, 228104 (2004).
- [16] O. Teschke and E. F. de Souza, *Appl. Phys. Lett.* **82**, 1126 (2003).
- [17] M. Ahmad, W. Gu, T. Geyer, and V. Helms, *Nat. Commun.* **2**, 261 (2011).
- [18] H. Itoh and H. Sakuma, *J. Chem. Phys.* **142**, 184703 (2015).
- [19] A. Schlaich, E. W. Knapp, and R. R. Netz, *Phys. Rev. Lett.* **117**, 048001 (2016).
- [20] C. Zhang, *J. Chem. Phys.* **148**, 156101 (2018).
- [21] L. Fumagalli, A. Esfandiari, R. Fabregas, S. Hu, P. Ares, A. Janardanan, Q. Yang, B. Radha, T. Taniguchi, K. Watanabe, G. Gomila, K. S. Novoselov, and A. K. Geim, *Science* **360**, 1339 (2018).
- [22] J. D. Weeks, D. Chandler, and H. C. Andersen, *J. Chem. Phys.* **54**, 5237 (1971).
- [23] S. Sarupria and S. Garde, *Phys. Rev. Lett.* **103**, 037803 (2009).
- [24] H. J. C. Berendsen, J. R. Grigera, and T. P. Straatsma, *J. Phys. Chem.* **91**, 6269 (1987).
- [25] L. Hong and J. Lei, *J. Polym. Sci. B Polym. Phys.* **47**, 207 (2009).
- [26] T. Darden, D. York, and L. Pedersen, *J. Chem. Phys.* **98**, 10089 (1993).
- [27] J. P. Ryckaert, G. Ciccotti, and H. J. C. Berendsen, *J. Comput. Phys.* **23**, 327 (1977).
- [28] D. A. Case *et al.*, *AMBER9* (University of California, San Francisco, 2006).
- [29] See Supplemental Material at <http://link.aps.org/supplemental/10.1103/PhysRevLett.121.206002> for Supplemental Figs. S1–S4.
- [30] J. G. Kirkwood, *J. Chem. Phys.* **7**, 911 (1939).
- [31] H. Fröhlich, *Theory of Dielectrics: Dielectric Constant and Dielectric Loss*, 2nd ed. (Clarendon, Oxford, 1958).
- [32] G. King, F. S. Lee, and A. Warshel, *J. Chem. Phys.* **95**, 4366 (1991).
- [33] H. Acharya, S. Vembanur, S. N. Jamadagni, and S. Garde, *Faraday Discuss.* **146**, 353 (2010).
- [34] M. R. Reddy and M. Berkowitz, *Chem. Phys. Lett.* **155**, 173 (1989).
- [35] A. Luzar and D. Chandler, *J. Chem. Phys.* **98**, 8160 (1993).
- [36] C. Zhang, F. Gygi, and G. Galli, *J. Phys. Chem. Lett.* **4**, 2477 (2013).
- [37] S. De Luca, S. K. Kannam, B. D. Todd, F. Frascoli, J. S. Hansen, and P. J. Davis, *Langmuir* **32**, 4765 (2016).
- [38] S. Kumar, D. Bouzida, R. H. Swendsen, P. A. Kollman, and J. M. Rosenberg, *J. Comput. Chem.* **13**, 1011 (1992).
- [39] M. Takano, in *Role of Water in ATP Hydrolysis Energy Transduction by Protein Machinery*, edited by M. Suzuki (Springer, Singapore, 2018), pp. 113–122.
- [40] A. A. Bogan and K. S. Thorn, *J. Mol. Biol.* **280**, 1 (1998).
- [41] O. Keskin, A. Gursoy, B. Ma, and R. Nussinov, *Chem. Rev.* **108**, 1225 (2008).